

Diagnosis of breast cancer using fluorescence and diffuse reflectance spectroscopy: a Monte-Carlo-model-based approach

Changfang Zhu

University of Wisconsin-Madison
Department of Electrical and Computer Engineering
Madison, Wisconsin 53705
E-mail: czhu@cae.wisc.edu

Gregory M. Palmer

Duke University
Department of Radiation Oncology
Durham, North Carolina 27710

Tara M. Breslin

University of Michigan
Division of Surgical Oncology
Ann Arbor, Michigan 48109

Josephine Harter

University of Wisconsin
Department of Pathology
Madison, Wisconsin 53705

Nirmala Ramanujam

Duke University
Department of Biomedical Engineering
Durham, North Carolina 27708

Abstract. We explore the use of Monte-Carlo-model-based approaches for the analysis of fluorescence and diffuse reflectance spectra measured *ex vivo* from breast tissues. These models are used to extract the absorption, scattering, and fluorescence properties of malignant and nonmalignant tissues and to diagnose breast cancer based on these intrinsic tissue properties. Absorption and scattering properties, including β -carotene concentration, total hemoglobin concentration, hemoglobin saturation, and the mean reduced scattering coefficient are derived from diffuse reflectance spectra using a previously developed Monte Carlo model of diffuse reflectance. A Monte Carlo model of fluorescence described in an earlier manuscript was employed to retrieve the intrinsic fluorescence spectra. The intrinsic fluorescence spectra were decomposed into several contributing components, which we attribute to endogenous fluorophores that may present in breast tissues including collagen, NADH, and retinol/vitamin A. The model-based approaches removes any dependency on the instrument and probe geometry. The relative fluorescence contributions of individual fluorescing components, as well as β -carotene concentration, hemoglobin saturation, and the mean reduced scattering coefficient display statistically significant differences between malignant and adipose breast tissues. The hemoglobin saturation and the reduced scattering coefficient display statistically significant differences between malignant and fibrous/benign breast tissues. A linear support vector machine classification using (1) fluorescence properties alone, (2) absorption and scattering properties alone, and (3) the combination of all tissue properties achieves comparable classification accuracies of 81 to 84% in sensitivity and 75 to 89% in specificity for discriminating malignant from nonmalignant breast tissues, suggesting each set of tissue properties are diagnostically useful for the discrimination of breast malignancy. © 2008 Society of Photo-Optical Instrumentation Engineers. [DOI: 10.1117/1.2931078]

Keywords: fluorescence; diffuse reflectance; spectroscopy; intrinsic fluorescence; optical property; Monte Carlo; breast cancer.

Paper 07202RR received May 31, 2007; revised manuscript received Dec. 16, 2007; accepted for publication Jan. 11, 2008; published online May 30, 2008.

1 Introduction

Fluorescence and diffuse reflectance spectroscopy in the ultraviolet-visible (UV-VIS) spectrum, are increasingly being investigated for breast cancer diagnosis.¹⁻¹⁵ This technology is cost-effective, and can be deployed through fiber optic probes to quickly, nondestructively, and quantitatively detect the structural, physiological, and biochemical changes that are associated with the progression of disease. Several studies have demonstrated that there are significant differences in the fluorescence^{1-3,5,7,9,11} and diffuse reflectance^{4,13-17} spectra of

normal, benign, and malignant breast tissues, which could be used for the diagnosis of breast malignancy.

In most previous studies, fluorescence^{1-3,5,7,9,11} and/or diffuse reflectance spectra^{1,4,5,8,13,15} of breast tissues were analyzed using empirical methods, in which the spectral intensities and/or line shapes were examined to extract spectral patterns (such as intensities, ratio of intensities, or principal components) that consistently discriminate between malignant and nonmalignant tissues. For example, in one of the first reported studies, Alfano et al.¹¹ used the ratio of fluorescence intensities at 340 and 440 nm, excited at 300 nm, to distinguish malignant from normal breast tissues. While several studies^{1-4,7,11,13} examined the spectral intensities, there are

Address all correspondence to Nimmi Ramanujam, Dept. Biomedical Engineering, Duke University, 136 Hudson Hall, Box 90281, Campus, Durham, NC 27708-0281; Tel: (919) 660-5307; Fax: (919) 684-4488; E-mail: nimmi@duke.edu

other studies where spectral line shapes were explored for breast cancer diagnosis. For example, Palmer et al.⁵ employed principal component analysis (PCA) to extract a set of principal components that dramatically reduced the spectral data dimension with minimal information loss, and showed that a subset of principal components obtained from diffuse reflectance spectra and fluorescence spectra at excitation wavelengths of 300, 400, 420, and 460 nm displayed the statistically most significant differences between malignant and nonmalignant breast tissues. The preceding collection of studies examined spectral intensities or line shapes of turbid tissue fluorescence and/or diffuse reflectance spectra. Although empirical analyses can reveal important spectroscopic features for tissue characterization and disease diagnosis, they do not relate the measured spectra directly to the physically meaningful information that are contained in the spectra.

The diffuse reflectance spectrum reflects the absorption and scattering properties of the tissue. The absorption coefficient is directly related to the concentration of physiologically relevant absorbers in the tissue such as oxygenated and deoxygenated hemoglobin. The scattering coefficient reflects the size and density of scattering centers in tissue, such as cells and nuclei. The fluorescence spectrum contains biochemical information about a number of molecules that are relevant to the structural properties of tissues or respiratory metabolism of cells. However, there are distortions in the fluorescence spectra due to the interplay of tissue absorption and scattering, which makes it difficult to interpret the biochemically relevant information contained in the fluorescence. Extracting and quantitatively assessing the intrinsic and physically meaningful information from the fluorescence and diffuse reflectance measurements will provide insight into the biochemical, physiological and morphological changes that take place during the progression of disease.

Several studies have been reported in which the absorption and scattering properties were quantified from diffuse reflectance spectra to characterize breast tissues. Ghosh et al.¹⁶ used a model based on the standard diffusion approximation to extract the absorption and scattering coefficients from spatially resolved diffuse reflectance measurements of human breast tissue samples. They showed that malignant tissues had increased absorption and scattering relative to nonmalignant breast tissues. However, they did not report the classification accuracy for diagnosing breast cancer based on the parameters extracted from the model. More recently our group, in two independent studies^{17,18} applied a Monte-Carlo-based inverse model for the extraction of absorption and scattering properties from the diffuse reflectance spectra of malignant and nonmalignant breast tissues. Both studies showed that malignant tissues have decreased hemoglobin saturation and increased mean reduced scattering coefficients compared to nonmalignant tissues. Classification based on machine learning using these absorption and scattering properties as inputs achieved an unbiased sensitivity and specificity of 82 and 92%, respectively, in the study by Palmer et al.,¹⁸ and 86 and 80%, respectively, in the study by Zhu et al.¹⁷, for discriminating between malignant and nonmalignant breast tissues.

For fluorescence, a number of studies¹⁹⁻²⁵ have been carried out to disentangle the effects of absorption and scattering from the measured fluorescence spectrum to recover the intrinsic fluorescence of the tissue. The intrinsic fluorescence is

due only to fluorophores present in the medium, from which fluorophore concentrations can be extracted using simple analytical models. A majority of these studies used analytical methods to derive mathematical expressions for the intrinsic fluorescence, from which the intrinsic fluorescence spectrum can be calculated.^{20-22,24,25} These methods are based on the diffusion equation and thus are valid for a limited range of absorption and scattering, not flexible in their applicability to various probe geometries or require extensive empirical calibration. Biswal et al.²³ proposed a method that was based on simultaneous measurements of polarized fluorescence and polarized elastic scattering spectra, and turbidity-free fluorescence was obtained by normalizing the polarized fluorescence spectrum by the polarized elastic scattering spectrum. Our group¹⁹ developed a fluorescence model based on scalable Monte Carlo simulations, which is capable of extracting the intrinsic fluorescence spectra of a turbid medium, and is applicable for a wide range of optical properties and, in principle, any illumination-collection geometry. The details of the model and its validation in synthetic phantoms are described in the preceding companion manuscript.²⁶ This paper uses the model to recover the intrinsic fluorescence of human breast tissues and to extract the relative fluorescence contribution of individual fluorescing components present in malignant and nonmalignant breast tissues.

The specific goals of this study were to (1) apply Monte-Carlo-model-based approaches developed by our group for the analysis of both fluorescence and diffuse reflectance spectra to extract the intrinsic fluorescence, absorption, and scattering properties of breast tissues and (2) test the diagnostic value of these intrinsic tissue properties for discriminating malignant from nonmalignant breast tissues. This work is distinct from previous publications by our group^{5,17,18} in that first, it reports on the application of a new fluorescence model to recover the intrinsic fluorescence and then extract the contributions of individual fluorescing components that may relate to intrinsic fluorophores in the breast; second, it compares the merits of the extracted fluorescence properties versus the tissue absorption and scattering properties for diagnosing breast cancer; and finally, it demonstrates the consistency of our model-based approach for the analysis of diagnostically useful information contained in fluorescence and diffuse reflectance spectra measured with two different instruments and probe geometries.

2 Methods

2.1 Sample Collection

Three sets of breast tissue samples were obtained from patients undergoing either breast cancer surgery (lumpectomy or mastectomy) or breast reduction surgery in two independent breast studies; both were approved by the Institutional Review Board at the University of Wisconsin, Madison. The two studies followed similar protocols for tissue handling and spectral measurements. In both studies, fluorescence and diffuse reflectance spectra were measured from freshly excised breast tissue samples immediately after excision. For tissue specimens obtained from cancer surgery, optical measurements were made at a cancerous site and a remote normal tissue site, and for tissue specimens obtained from breast reduction surgery, optical measurements were attempted at a fibroglandular

site and an adipose site. The tissue measurement and the handling protocol for the first breast study were described in detail elsewhere,^{1,17} and that for the second breast study can also be found in an earlier publication.⁵ Accompanying histological diagnoses were obtained for each tissue specimen from microscopic evaluation of hematoxylin and eosin (H&E) sections within a depth of 2 mm from the probe-tissue contact surface (marked by an ink spot). The breast tissue specimens were broadly categorized as malignant, benign, fibrous, and adipose. When malignancy presented anywhere within the depth of histological evaluation, the sample diagnosis was designated as being malignant. If a benign or normal sample exhibited heterogeneous tissue composition, the sample histology was designated to be the predominant tissue type immediately below the tissue surface where the optic probe was placed. In addition, the percent adipose, fibroconnective, and percent glandular tissue content within the region of interest (i.e., the 2-mm depth in the histological section) was quantified in all breast reduction surgery samples.

In the first study,¹⁷ fluorescence and diffuse reflectance spectroscopy was performed on 18 breast reduction patients and 45 cancer patients. According to the type of surgery, tissue samples were divided into two sets: the first set (set 1) contained only normal samples from healthy women undergoing breast reduction surgery, and the second (set 2) contained both cancerous and normal samples from cancer patients. A total of 64 normal samples were collected from the 18 breast reduction patients, however, 3 samples had to be excluded due to saturation in the spectral measurements, resulting in a total of 61 samples including 22 fibroglandular and 39 adipose samples in set 1. A total of 96 breast samples were collected from the 45 cancer patients, among which 13 samples had to be excluded from further analysis, due to either saturation of the measured spectra or due to the visible presence of lymphazurin on the measurement site. Thus, a total of 83 tissue samples, including 37 malignant, 2 benign, 6 fibrous, and 38 adipose samples were included in set 2 for further analysis.

In the second study,⁵ a total of 56 tissue samples were obtained from 32 cancer or breast reduction patients, however, 15 samples had to be excluded because they were measured with a demo instrument and the calibration information needed for the model analysis was not available. Thus, a total of 41 samples obtained in the second breast study, including 17 malignant, 4 benign, 6 fibrous, and 14 adipose breast tissues, were included in set 3.

Set 1 was used to carry out a correlation analysis between the tissue properties extracted from the model-based approach and histological parameters including percent adipose, fibroconnective, and glandular content in normal breast tissues from healthy women. Sets 2 and 3 were used in the discrimination analysis for the purpose of diagnosing breast cancer. Combining sets 2 and 3 yielded a sample size of 54 malignant, 6 benign, 12 fibrous, and 52 adipose tissues. Table 1 displays the histological break down of the breast tissue samples in this study.

2.2 Fluorescence and Diffuse Reflectance Measurements

In the two breast studies, different spectrometers and probe geometries were used for spectral measurements, both of

Table 1 Histological break down of the breast tissue samples examined in this study.

Type and Subtype	Set 1	Set 2	Set 3	Sets 2 and 3
Total malignant		37	17	54
Invasive ductal carcinoma (IDC)		29	15	44
Invasive lobular carcinoma (ILC)		2	2	4
Ductal carcinoma <i>in situ</i> (DCIS)		2	0	2
Lobular carcinoma <i>in situ</i> (LCIS)		2	0	2
Infiltrating tubulolobular		2	0	2
Total Nonmalignant		46	24	70
Benign		2	4	6
Fibro glandular	22	6	6	12
Adipose	39	38	14	52
Total samples	61	83	41	124

which were described in our earlier publications.^{1,5,17} In the first breast study (corresponds to sets 1 and 2), fluorescence and diffuse reflectance spectra were measured with a multi-wavelength optical spectrometer and the fiber optic probe used consists of a central illumination core and a surrounding collection ring.^{1,17} In the second breast study (corresponds to set 3), tissue spectral measurements were made using a Skin-skan spectrometer (JY Horiba, Edison, New Jersey) and a fiber optic probe that consists of a central collection core and a surrounding illumination ring.⁵ The measured fluorescence and diffuse reflectance spectra were calibrated in order to correct for the (1) background spectrum, (2) wavelength dependence, and (3) throughput of the system. A detailed description of instrument settings and calibrations for the fluorescence and diffuse reflectance measurements can be found in earlier publications.^{1,5,17} In both breast studies, fluorescence measurements covered excitation wavelengths of 300 to 460 nm in 20-nm increments, and emission wavelengths from 20 nm beyond each excitation wavelength up to 600 nm in increments of 5 nm. Diffuse reflectance measurements covered the wavelength range of 350 to 600 nm. Therefore, spectral analyses were carried out on the three sets of tissue spectra over these common wavelength ranges.

2.3 Extraction of Tissue Optical Properties

A scalable Monte Carlo inverse model of diffuse reflectance was used to extract the tissue optical properties. Details about the Monte-Carlo-based inverse model of diffuse reflectance can be found in previous publications.^{17,18,27} The accuracy of the inverse model was verified using experimental tissue phantom studies. The results indicated that for phantoms with a wide range of absorption coefficients (0 to 20 cm⁻¹) and reduced scattering coefficients (7 to 33 cm⁻¹), optical properties could be extracted within an average error of 3% for

phantoms containing hemoglobin and within 12% for phantoms containing nigrosin.²⁷ The diffuse reflectance spectra were fit to the Monte Carlo model in the wavelength range of 350 to 600 nm. The primary intrinsic absorbers in the model over this wavelength range were assumed to be oxygenated and deoxygenated hemoglobin and beta-carotene. Lymphazurin (Catalog no. 00592358, Tyco Healthcare, Mansfield, Massachusetts), a dye used to locate the sentinel lymph node during surgery, was included as an extrinsic absorber since it was found to be present in some of the tissue samples. A Gaussian function with a mean of 515 nm and a standard deviation of 13 nm was included as an additional absorbing component to account for a deviation in the fit between 500 and 530 nm, which was found in a large number of tissue samples. In addition, a baseline tissue absorption coefficient, describing protein absorption in the absence of blood²⁸ was added to the absorption coefficient calculated from the concentrations of the chromophores already mentioned. This baseline absorption is given by

$$\mu_a(\lambda) = a \left\{ 0.244 + 85.3 \exp \left[\frac{-(\lambda - 154)}{66.2} \right] \right\} (\text{cm}^{-1}), \quad (1)$$

where $\mu_a(\lambda)$ is the absorption as a function of wavelength, and a is the magnitude of the baseline absorption. The concentrations of each absorber and the magnitude a of the baseline absorption described in Eq. (1) were the free parameters related to absorption in the fit, which were extracted from the inversion process.

Note that for the first two data sets (sets 1 and 2), NADH was also included in the model as an absorber for the calculation of absorption coefficient, while this was not done for set 3. This discrepancy was due to the difference in model selection by individual researchers, and this was the only difference in the model parameters for fitting the diffuse reflectance spectra of sets 1 and 2 and set 3. However, the absorption due to NADH alone was found to account for only 0 to 3% on average of the total absorption across the wavelength range of 350 to 600 nm, with a mean of 0.4% and a standard deviation of 2%. This indicated that NADH did not contribute significantly to the absorption in this wavelength range, and the absorption and scattering properties obtained from the three sets of tissue spectra are still comparable. The absorption properties yielded from the model and used in further data analysis then include β -carotene concentration, total hemoglobin concentration, and hemoglobin saturation, and the latter two were calculated directly from the concentrations of oxygenated and deoxygenated hemoglobin.

For scattering, the refractive indices of the scatterers and the surrounding medium were fixed parameters and were assumed²⁹ to be 1.4 and 1.36, respectively. The scatterer size and density were the free parameters in the model related to scattering, and the scatterer size was constrained to be between 0.35 and 1.5 μm in diameter.³⁰ The wavelength-dependent scattering coefficient and anisotropy factor were calculated from scatterer size, density, and the refractive index mismatch between the scatterer and surrounding medium using the Mie theory for spherical particles. The mean reduced scattering coefficient was then calculated from the

wavelength-dependent scattering coefficient and anisotropy factor, and used to describe the bulk scattering properties of tissue.

Note that the tissue spectra of sets 2 and 3 were measured with different spectrometers and probes, and the spectral intensities were recorded on different scales. To directly compare the results obtained from the two data sets, it is important to remove the system dependency. The Monte Carlo inverse model of diffuse reflectance takes into account the specific probe geometry and incorporates a phantom calibration to account for the difference in system throughput thus allowing for a direct comparison of the absorption and scattering properties extracted from the two data sets.²⁷

2.4 Extraction of Intrinsic Fluorescence Spectra

A Monte-Carlo-based model of fluorescence was developed for the extraction of intrinsic fluorescence spectra of turbid tissues and is described in the preceding companion manuscript.¹⁹ This model is capable of removing the distorting effects of absorption and scattering and is valid for a wide range of optical properties. Using a phantom study, it was found that this model could recover the intrinsic fluorescence line shape and intensity of the tissue phantoms within an average percent error of less than 10%, as described in the companion manuscript.¹⁹ The Monte Carlo model simulates photon propagation (including both incident photons and fluorescence reemission photons) within a turbid medium, given a set of known absorption and scattering coefficients and illumination-collection geometry. In our approach, the set of absorption and scattering coefficients of tissue were derived from the concomitantly measured diffuse reflectance spectrum using the Monte-Carlo-based inverse model of diffuse reflectance, which was described in the previous section. Next, these optical properties were used in the scalable Monte Carlo model of fluorescence to account for the effects of absorption and scattering on the fluorescence emission.

In this study, fluorescence spectra within an excitation wavelength range of 340 to 460 nm and an emission wavelength range of 350 to 600 nm were processed with the model to retrieve the intrinsic fluorescence, since diffuse reflectance was measured within 350 to 600 nm and absorption and scattering properties can be determined only for this wavelength range. The absorption and scattering coefficients at 340 nm were determined using the chromophore concentrations, scatterer size, and scatterer density extracted from the diffuse reflectance spectra within 350 to 600 nm. Inputs into the fluorescence model include the absorption and scattering coefficients at both the excitation and emission wavelengths. The model then used a scaling technique reported by Graaff et al.³¹ to simulate the propagation of photons in a turbid medium with these absorption and scattering properties. A correction curve was generated from the output of the Monte Carlo simulation, which accounts for the effects of absorption and scattering in the medium at both excitation and emission wavelengths, as well as the collection efficiency defined by the specific probe geometry used. This correction curve corresponds to the denominator in Eq. (8) in the companion manuscript.¹⁹ The measured tissue fluorescence spectra were then divided point by point by the correction curve to retrieve the intrinsic fluorescence spectra independent of the absorp-

tion and scattering properties of tissue and probe geometry.

The Monte Carlo model also includes¹⁹ a scaling factor S , which accounts for the difference in magnitude between the Monte Carlo simulations and the measured result. This factor can be determined by comparing the measured and simulated fluorescence of a reference phantom with known optical properties, and must be known to compare, on an absolute scale, the intrinsic fluorescence measured with the two different instruments and probe geometries. In this study, the intrinsic fluorescence spectra of each tissue sample were normalized to the integrated intensity of the excitation-emission matrix (EEM), thus, the difference in magnitude between the two sets of tissue spectra (sets 2 and 3) and the Monte Carlo simulations are removed, and a direct comparison of the relative (fractional) fluorescence contributions from individual fluorophores is possible.

2.5 Extraction of Relative Fluorescence Contribution from Individual Fluorophores

The intrinsic fluorescence spectrum can be viewed as a linear combination of the fluorescence emission by one or more contributing fluorescent components (fluorophores). A multivariate curve resolution (MCR) method³² was used to decompose the intrinsic tissue fluorescence into several spectral profiles of the contributing components. MCR refers to a group of techniques that intend the recovery of response profiles, e.g., spectra, of the components in an unresolved mixture when no or limited prior information is available about the nature and composition of these mixtures. In this study, three components were assumed to contribute to the tissue fluorescence within excitation wavelength range of 340 to 460 nm and emission wavelength range of 350 to 600 nm, as there are three visible fluorescence peaks present in tissue EEMs in these spectral ranges. An MCR toolbox available from the Chemometrics Group at the University of Barcelona³² was used to extract the relative fluorescence contribution of each component, as well as their intrinsic spectral line shape.

Prior to MCR analysis, the intrinsic fluorescence spectra of each tissue sample were normalized to the integrated intensity over the entire EEM, that is, the fluorescence intensities over all excitation-emission wavelength pairs sum up to unity. This normalization removed the patient-to-patient variation and the difference in the magnitude of fluorescence spectra measured with different spectrometers and probe geometries. MCR analysis was then carried out on the normalized fluorescence EEM, and the intrinsic tissue fluorescence can be represented as:

$$F_{\text{tissue}}(\lambda_{\text{ex}}, \lambda_{\text{em}}) = \alpha_1 F_1(\lambda_{\text{ex}}, \lambda_{\text{em}}) + \alpha_2 F_2(\lambda_{\text{ex}}, \lambda_{\text{em}}) + \alpha_3 F_3(\lambda_{\text{ex}}, \lambda_{\text{em}}) + \varepsilon(\lambda_{\text{ex}}, \lambda_{\text{em}}),$$

where α_i represents the contribution and $F_i(\lambda_{\text{ex}}, \lambda_{\text{em}})$ represents the intensity of fluorescence from the i 'th component at excitation wavelength of λ_{ex} , and emission wavelength of λ_{em} , and $\varepsilon(\lambda_{\text{ex}}, \lambda_{\text{em}})$ is the residual component. In the MCR process, the basis fluorescence profile of each contributing component was normalized to have a peak of unity. Since all spectra were normalized to the integrated intensity within an EEM, α_i then represents the fractional fluorescence contribution from an individual component to that sample. Note that

the value of α_i is related to the quantum yield and absorption coefficient (a function of fluorophore concentration and extinction coefficient) of the individual fluorescing component at the excitation wavelength. The quantities α_i are the fluorescence properties that we obtained from the fluorescence model analysis.

2.6 Correlation Between Extracted Tissue Properties and Histological Tissue Composition

The extracted optical properties and fluorescence contributions were evaluated for their correlation with the histological tissue composition in the normal tissues obtained from breast reduction surgery (set 1). The tissue composition within the sensing volume of the optical measurements was recorded as %adipose, %fibro-connective, and %glandular. Spearman correlations were used to determine the correlation coefficients and p values for the relationship between the extracted tissue properties and the histological tissue composition.

2.7 Statistical Analysis and Classification Using Fluorescence Properties

The tissue absorption and scattering properties and fluorescence contributions of individual components extracted from the tissue sets 2 and 3 were pooled together for the purpose of discriminating malignant from nonmalignant breast tissues. A Wilcoxon rank-sum test was performed to identify which extracted features from the diffuse reflectance and fluorescence spectra show statistically significant differences between malignant and nonmalignant breast tissues. The optical properties and/or fluorophore contributions that displayed statistically significant differences were input to a linear support vector machine (SVM) classifier to test the diagnostic accuracy of using these tissue properties for discriminating malignant from nonmalignant breast tissues. Classification was carried out on (1) absorption and scattering properties only, (2) fluorophore contributions only, and (3) combination of fluorophore contribution with absorption and scattering properties. For each case, two cross-validation schemes, i.e., holdout validation and leave-one-out cross-validation, were employed to perform an unbiased evaluation of the classification accuracy. In the holdout validation, the entire data set was randomly divided into training and testing sets, with each set containing half of the breast samples of each tissue type (i.e., 50% of the total malignant, 50% of the total fibrous/benign, and 50% of the total adipose tissue samples). Such a random partition was repeated 20 times, and the average classification accuracy was evaluated. In the leave-one-out cross-validation, a single sample was used as the testing data and the remaining samples were used as the training data. This was repeated such that each sample was used once as the test data.

3 Results

Figure 1 shows the average absorption coefficient [Fig. 1(a)] and average reduced scattering coefficient [Fig. 1(b)] as a function of wavelength, for malignant ($n=37$), fibrous/benign ($n=8$), and adipose ($n=38$) tissues in sample set 2. For all tissue types, significant hemoglobin absorption was observed at approximately 420, 530, and 575 nm. Adipose tissues displayed an additional absorption band in the wavelength range of 440 to 500 nm. This absorption band is primarily attributed

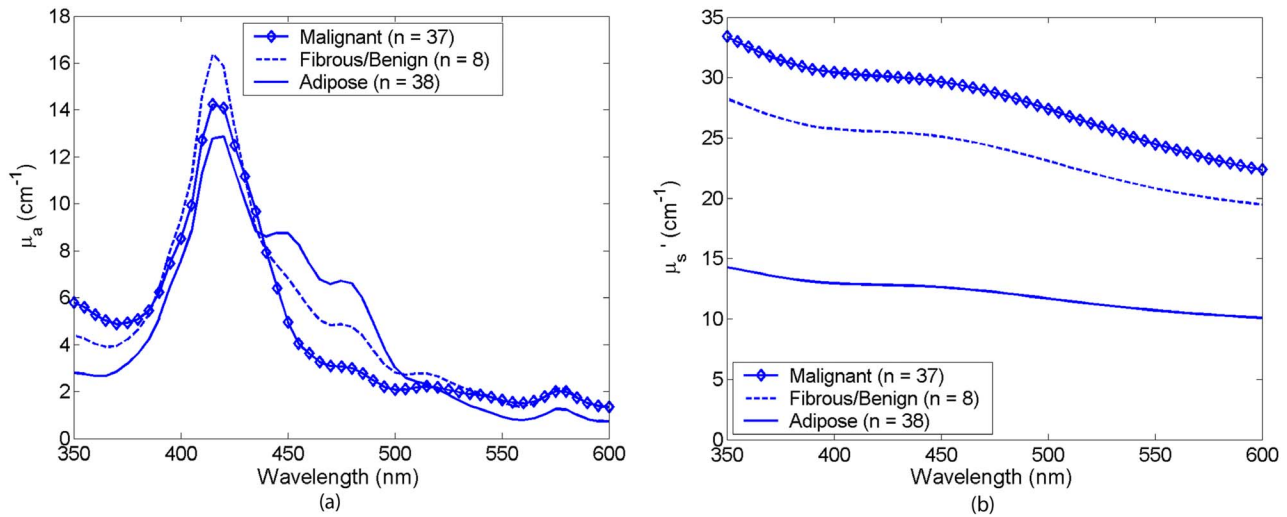


Fig. 1 (a) Average absorption coefficient and (b) average reduced scattering coefficient as a function of wavelength, for malignant ($n=37$), fibrous/benign ($n=8$) and adipose ($n=38$) tissues in sample set 2.

to beta-carotene, which is present primarily in fat or adipose tissues. The scattering coefficients of all tissue types decreased monotonically with increasing wavelength. The average absorption and reduced scattering coefficients of the three tissue types in sample set 3 displayed similar features, but are not shown here.

Figure 2 shows the representative raw [Fig. 2(a)] and intrinsic [Fig. 2(b)] EEMs of a malignant tissue sample, each normalized to the integrated intensity of the EEM and plotted on a log scale. In comparing the raw and intrinsic EEMs, the most obvious change is the disappearance of the fluorescence peak at the wavelength pair around (440, 510) nm in the intrinsic EEM. In addition, the dip shown in the raw EEM at around 420 nm, which is due to hemoglobin absorption, is also corrected for in the intrinsic EEM.

Figure 3 displays the average intrinsic fluorescence spectra obtained at excitation wavelength of 340 [Fig. 3(a)] and

360 nm [Fig. 3(b)] for malignant ($n=37$), fibrous/benign ($n=8$), and adipose ($n=38$) tissues in sample set 2. Malignant and fibrous/benign tissue samples share similar spectral profiles and displayed strong fluorescence at the emission wavelengths around 395 nm at 340-nm excitation and around 450 nm at 360-nm excitation. In adipose tissue samples, there was a weak presence of fluorescence at wavelengths around 395 nm, but strong fluorescence at the wavelengths between 450 and 500 nm. The shoulder at a wavelength of 420 nm in the spectra of malignant and fibrous/benign tissue samples are not fluorescence peaks but rather artifacts that may be introduced from the overcorrection of the Soret band of hemoglobin absorption. The average intrinsic fluorescence spectra of the three tissue types in sample set 3 (not shown here) displayed similar spectral features but the intensities were on a different scale.

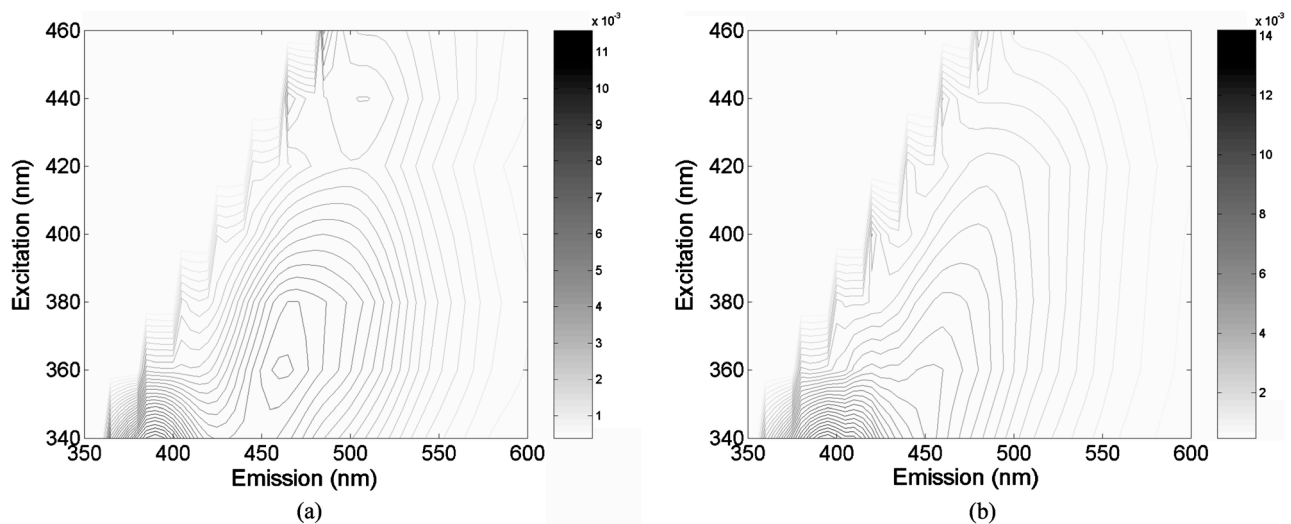


Fig. 2 (a) Raw and (b) intrinsic fluorescence EEMs of a representative malignant tissue sample, each normalized to the integrated intensity of the EEM and plotted on a log scale.

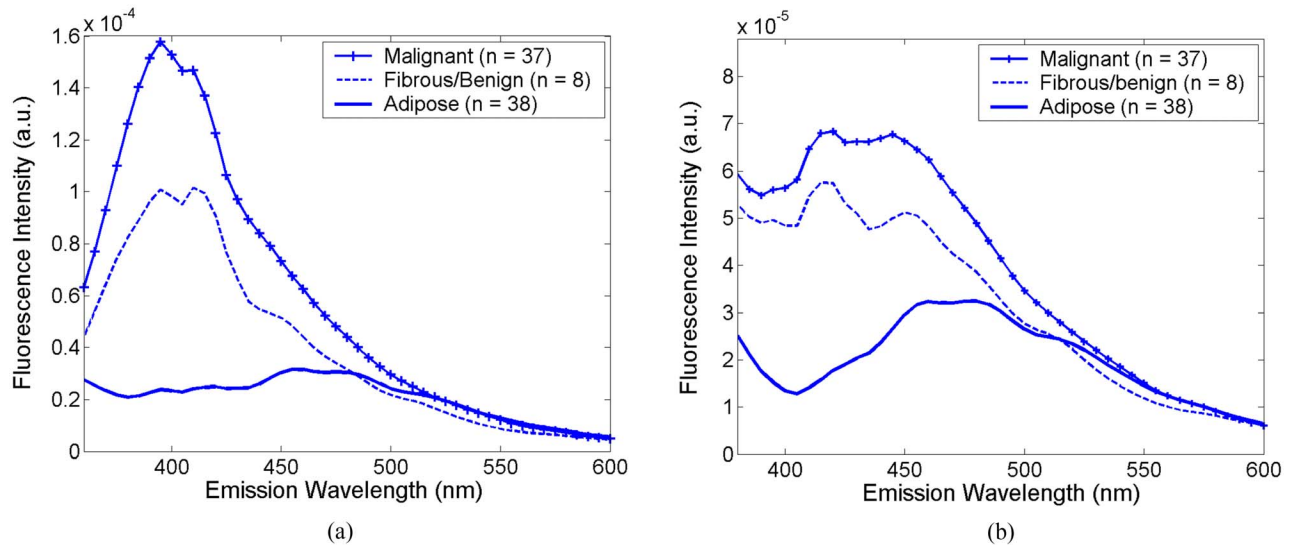


Fig. 3 Average intrinsic fluorescence spectra obtained at excitation wavelengths of (a) 340 and (b) 360 nm, for malignant ($n=37$), fibrous/benign ($n=8$), and adipose ($n=38$) tissues in sample set 2.

A three-component MCR analysis was carried out on the intrinsic fluorescence EEM to extract the relative contribution of the constituent fluorescing components, as well as their intrinsic spectral line shape. Figures 4(a) to 4(c) shows the EEMs of the three fluorescing components (denoted as F_1 , F_2 , and F_3) obtained from the MCR analysis on intrinsic EEMs of sample set 2. Each intrinsic tissue EEM is a linear combination of the component EEMs. These three components accounted for a vast majority of variance in the tissue EEMs, as the residual was only about 0.2% of the tissue EEM. The first component F_1 [Fig. 4(a)] displayed excitation-emission maximum at a wavelength pair of (340,395) nm. The second component F_2 [Fig. 4(b)] displayed strong fluorescence at the emission wavelengths ranging from 450 to 500 nm over an excitation range of 360 to 420 nm. The third component F_3 [Fig. 4(c)] had peak fluorescence at an emission wavelength of 480 nm at 340 to 360 nm excitation. This component was found to be prevalent in adipose tissues.

Table 2 shows the correlations between the extracted scattering, absorption and fluorescence (marked with *) properties and the constituent tissue composition, which were evaluated on breast tissues in sample set 1 (note: +, positive correlation; -, negative correlation; \emptyset , no significant correlation). Correlations were considered significant for $p < 0.01$. The mean reduced scattering coefficient, μ'_s and the fluorescence contribution from F_1 and F_2 were negatively correlated with %adipose, while positively correlated with %fibroconnective and %glandular tissue content. The β -carotene concentration and the fluorescence contribution of F_3 both had significant positive correlations with %adipose content, while they showed negative correlations with %fibroconnective and %glandular tissue content.

Table 3 shows the pairwise cross-correlation between extracted scattering, absorption (including baseline absorption component) and fluorescence (marked with *) properties of the combined sample sets (note: +, positive correlation; -, negative correlation; \emptyset , no significant correlation). Correla-

tion was evaluated using sample sets 2 and 3. Optical properties obtained from the diffuse reflectance did not show statistically significant correlations with each other. For fluorescence properties, the fluorescence contribution of F_3 was negatively correlated with that of F_1 ($r = -0.67$, $p < 1 \times 10^{-16}$) and F_2 ($r = -0.70$, $p < 1 \times 10^{-16}$). In addition, the mean reduced scattering coefficient was positively correlated with the fluorescence contribution of F_2 ($r = 0.23$, $p < 0.01$), while negatively correlated with the fluorescence contribution of F_3 ($r = -0.26$, $p < 0.005$). β -carotene concentration had a strong positive correlation with the fluorescence contribution of F_3 ($r = 0.67$, $p < 1 \times 10^{-16}$), and negative correlations with that of F_1 ($r = -0.56$, $p < 1 \times 10^{-10}$) and F_2 ($r = -0.38$, $p < 0.00005$). There was also a positive correlation between the total hemoglobin concentration and F_2 ($r = 0.23$, $p < 0.01$), and a negative correlation between hemoglobin saturation and F_1 ($r = -0.30$, $p < 0.001$). The baseline absorption component did not show statistically significant correlation with other extracted properties except for the fluorescence contribution of F_3 ($r = -0.23$, $p < 0.005$).

Figure 5 shows the bar graphs of β -carotene concentration [Fig. 5(a)], mean reduced scattering coefficient (mean μ'_s) [Fig. 5(b)], hemoglobin saturation (H_bO_2 %) [Fig. 5(c)] and relative fluorescence contribution of individual fluorescing components [Fig. 5(d)], as a function of tissue type. Data shown here were obtained from the combined sample sets (sets 2 and 3). β -carotene concentration [Fig. 5(a)] was statistically higher in adipose breast tissues compare to that in malignant ($p < 1 \times 10^{-10}$) and fibrous/benign breast tissues ($p < 0.001$). The mean reduced scattering coefficients μ'_s [Fig. 5(b)] of malignant tissues were higher than that of fibrous/benign ($p < 0.05$) and adipose breast tissues ($p < 1 \times 10^{-9}$). Hemoglobin saturation [Fig. 5(c)] was higher in both fibrous/benign and adipose breast tissues in comparison to that in malignant tissues ($p < 0.0001$). In Fig. 5(d), it is

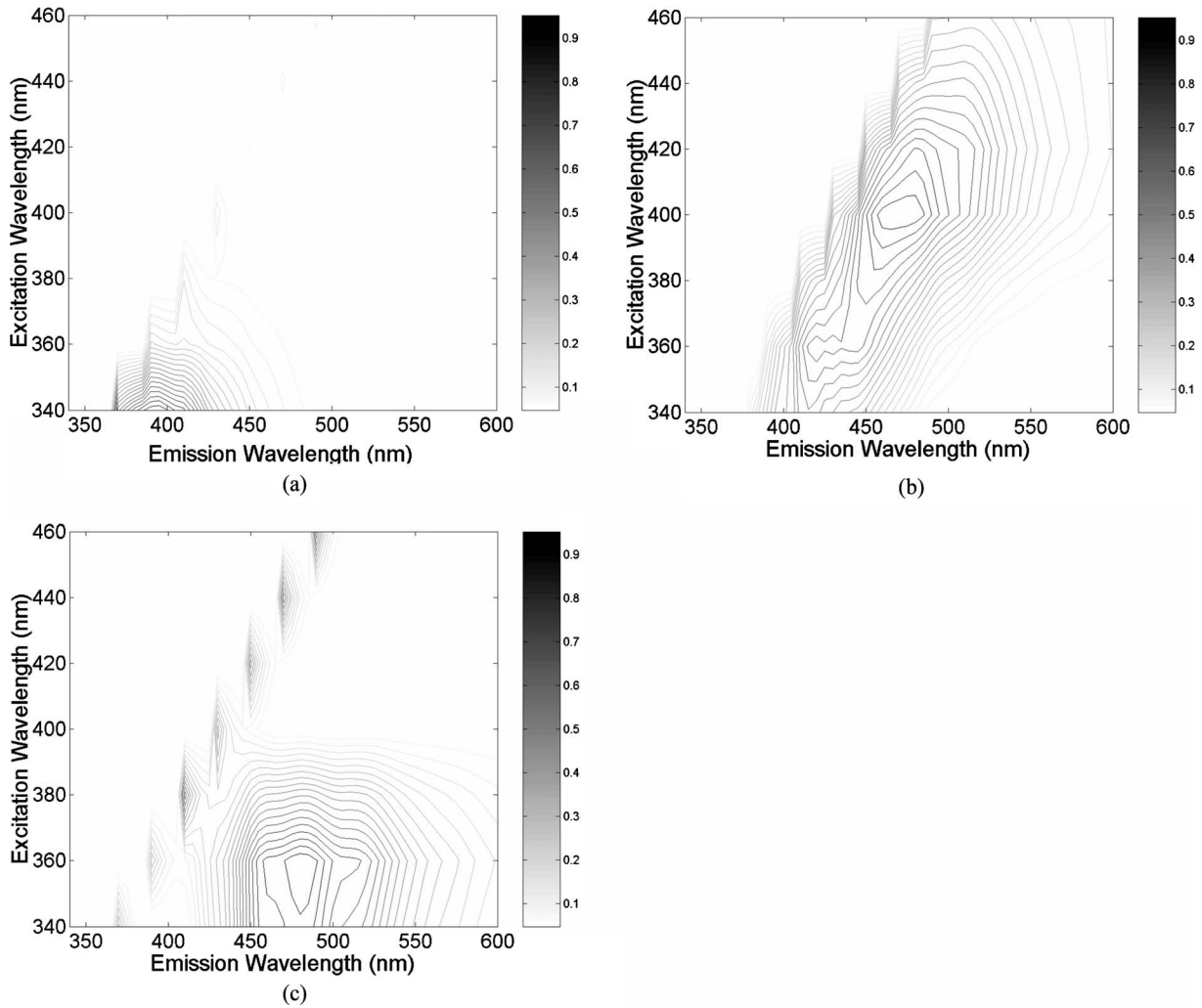


Fig. 4 EEMs of fluorescing components (a) F_1 , (b) F_2 , and (c) F_3 obtained from a three-component MCR analysis on intrinsic EEMs of sample set 2.

Table 2 Correlations between the extracted scattering, absorption and fluorescence (marked with +) properties and the histological tissue composition, evaluated on breast tissues in sample set 1.

	Percent Adipose	Percent Fibroconnective	Percent Glandular
Mean reduced scattering coefficient μ'_s (cm^{-1})	-0.61 (-)	0.63 (+)	0.39 (+)
β -carotene concentration (μM)	0.66 (+)	-0.61 (-)	-0.64 (-)
Total hemoglobin concentration (μM)	\emptyset	\emptyset	\emptyset
Hemoglobin saturation (%)	\emptyset	\emptyset	\emptyset
F_1 contribution*	-0.42 (-)	0.37 (+)	0.44 (+)
F_2 contribution*	-0.80 (-)	0.81 (+)	0.58 (+)
F_3 contribution*	0.83 (+)	-0.82(-)	-0.65 (-)
Baseline absorption	\emptyset	\emptyset	\emptyset

(Note +: positive correlation; -: negative correlation; \emptyset : no significant correlation); correlations were considered significant for $p < 0.01$.

Table 3 Pairwise cross-correlation between extracted scattering, absorption (including baseline absorption component) and fluorescence (marked with *) properties.

	μ'_s	β -Carotene	Total Hb	HbO ₂ %	F_1^*	F_2^*	F_3^*	Baseline
μ'_s								
β -carotene	∅							
Total Hb	∅	∅						
HbO ₂ %	∅	∅	∅					
F_1^*	∅	-0.56	0	-0.30				
F_2^*	+0.23	-0.38	+0.23	∅	0			
F_3^*	-0.26	+0.67	∅	∅	-0.67	-0.70		
Baseline	∅	∅	∅	∅	∅	∅	-0.23	

Note: μ'_s : mean reduced scattering coefficient; β -carotene: β -carotene concentration; total Hb: total hemoglobin concentration; HbO₂%: hemoglobin saturation; F_1^* , F_2^* , and F_3^* : fluorescence contribution of F_1 , F_2 , and F_3 ; +, positive correlation; -, negative correlation; ∅: no significant correlation.

shown that relative fluorescence contribution of F_1 and F_2 were higher in malignant and fibrous/benign tissues compare to that in adipose tissues ($p < 0.0001$), while the inverse trend was observed for F_3 ($p < 1 \times 10^{-7}$).

Table 4 lists the results from Wilcoxon rank-sum test on extracted absorption, scattering, and fluorescence properties for malignant versus nonmalignant and malignant versus fibrous/benign breast tissues (properties are listed in the order of decreased p value for differentiating between malignant and non-malignant tissues, and fluorescence properties are marked with *). The difference in data distribution is considered statistically significant for $p < 0.05$. All extracted properties, except for total hemoglobin concentration and the baseline absorption component, displayed statistically significant differences between malignant and non-malignant breast tissues ($p < 0.0001$). However, only hemoglobin saturation and the mean reduced scattering coefficient displayed statistically significant difference between malignant and fibrous/benign breast tissues. This suggests that the fluorescence contrast shown between malignant and nonmalignant breast tissues may be primarily associated with the differences between malignant and adipose tissues.

Table 5 shows the results from the (a) holdout validation and (b) leave-one-out cross validation of a linear SVM classification on the combined data sets for discriminating malignant from non-malignant breast tissue samples using: (1) absorption and scattering properties only; (2) fluorescence properties only; and (3) combination of fluorescence, absorption, and scattering properties that show statistically significant differences between malignant and non-malignant breast tissues. The classification rate (C rate), sensitivity and specificity were averaged over repeated training-and-testing trials. In holdout validation [Table 5(a)], classification using absorption and scattering properties alone provided an average sensitivity and specificity of 82.6 and 90.1% respectively in training, and 81.7 and 88.6%, respectively, in testing for discriminating malignant from nonmalignant breast tissues. The classification using fluorescence properties alone yielded

slightly higher sensitivity but relatively lower specificity (average SE and SP of 83.4 and 78.7%, respectively, in training, and 82.6 and 75.7%, respectively, in testing) compared to that achieved using absorption and scattering properties alone. It was also shown that combining fluorescence properties with absorption and scattering properties for classification slightly improved the diagnostic accuracy, and the average sensitivity and specificity were improved to 87.6 and 90.6% respectively in training, and 83.9 and 88.6% in testing, for discriminating malignant from non-malignant breast samples. In the leave-one-out cross-validation [Table 5(b)], the classification accuracy for the three cases were comparable to those yielded from the holdout validation. To summarize, the classification using absorption and scattering properties alone and that using combined fluorescence, absorption and scattering properties yielded similar classification accuracy, and both outperformed the classification using fluorescence properties alone.

Table 6 lists the number of tissue samples from each tissue type that were frequently (repeatedly) misclassified in the SVM classification using the three sets of inputs: (1) absorption and scattering properties only; (2) fluorescence properties only; and (3) the combination of fluorescence, absorption, and scattering properties. The sample number for each of the misclassified tissue samples is listed in parentheses to show samples that were misclassified by more than one algorithm. The majority of misclassified malignant tissues had IDC. DCIS, ILC, and LCIS constitute 25 to 40% of the misclassified malignant samples. This may be partly attributed to the fact that these subtypes of malignancy only account for a very small portion of the malignant samples and may be underrepresented in this data set. Among the misclassified malignant samples, the same LCIS and two IDCs were consistently misclassified using both the fluorescence only and the reflectance only algorithms. The ILCs were misclassified in the reflectance only algorithm, while DCIS was misclassified in the fluorescence only algorithm. More fibrous and benign samples were misclassified when using fluorescence properties alone for classification versus using reflectance properties, and these

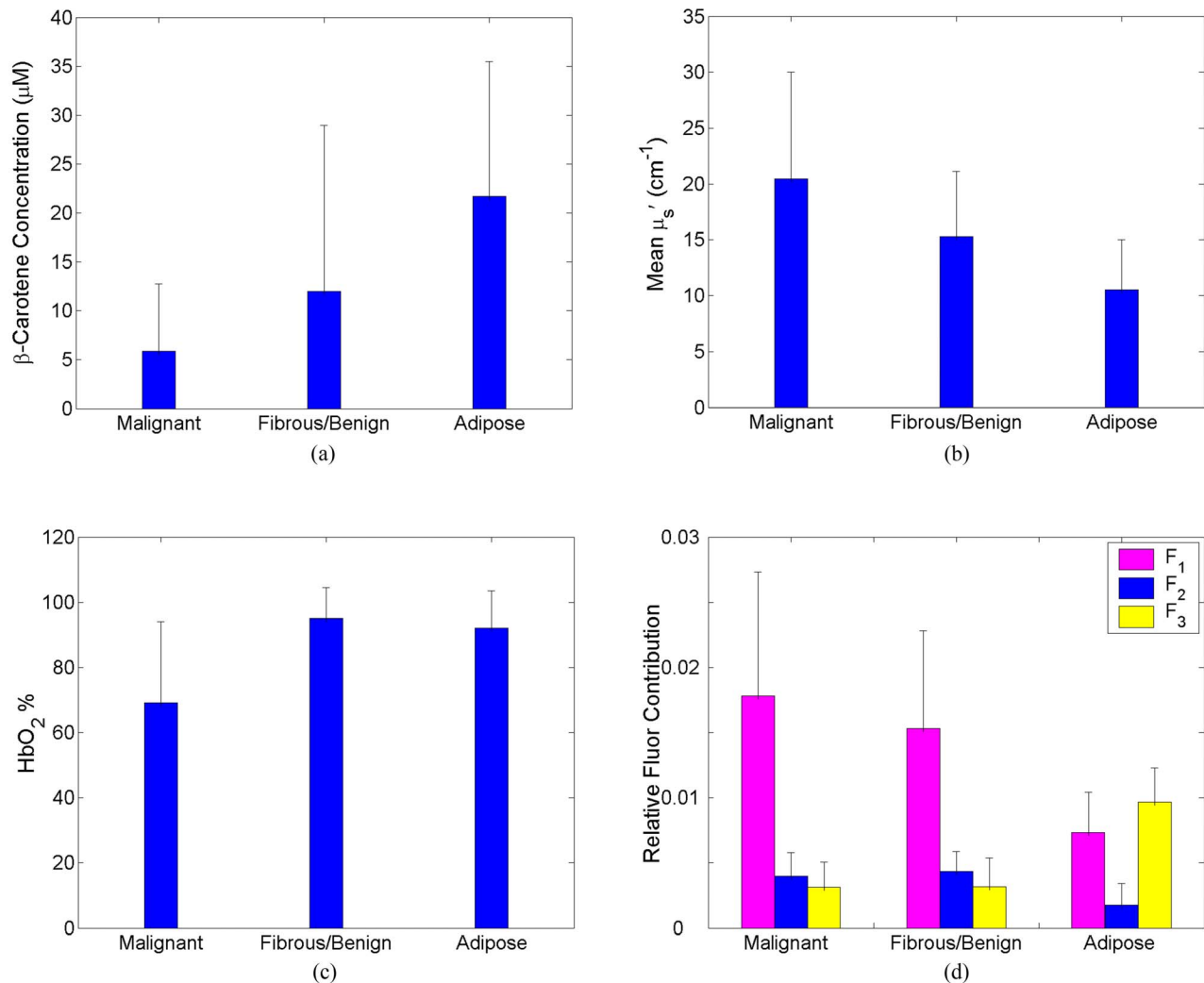


Fig. 5 Bar graphs of (a) β -carotene concentration, (b) mean reduced scattering coefficient (mean μ'_s), (c) hemoglobin saturation ($\text{HbO}_2\%$), and (d) relative fluorophore contribution of individual fluorophores (F_1 , F_2 , and F_3), as a function of tissue type for samples combined from sets 2 and 3.

fibrous or benign samples accounted for the majority of misclassified non-malignant samples. Two of the benign samples, two of the fibro glandular samples and one of the adipose samples were consistently misclassified in reflectance only and fluorescence only classifications. For both malignant and non-malignant cases, most samples misclassified using combined tissue properties overlapped with those misclassified using the reflectance only algorithm.

4 Discussion

In this paper, we explored the use of Monte-Carlo-model-based approaches to extract a set of tissue properties, including intrinsic fluorophore contributions and absorption and scattering properties, which include β -carotene concentration, total hemoglobin concentration, hemoglobin saturation, and mean reduced scattering coefficient from fluorescence and diffuse reflectance measurements of malignant and nonmalignant breast tissues. For normal samples obtained from breast reduction patients, the mean reduced scattering coefficient decreased with the %adipose tissue content, while it increased with the %fibroconnective and %glandular tissue content.

This agrees with findings from previously published studies. For example, Peters et al.¹⁴ estimated the reduced scattering coefficients at 540 nm for normal fibrous and normal adipose breast tissues and showed that fibrous tissues had higher reduced scattering coefficients as compared to adipose tissues. Cerussi et al.³³ and Durduran et al.³⁴ also showed in their studies that the scattering coefficients decreased with increasing body mass index (BMI). β -carotene concentration was positively correlated with the %adipose tissue content, while negatively correlated with %fibroconnective and %glandular tissue content. This agrees with the fact that the majority of body reserves of β -carotene are thought to be in adipose tissues.³⁵ In comparing the malignant, fibrous/benign, and adipose breast tissues, β -carotene had an increased concentration in adipose breast tissues compared to that of malignant ($p < 1 \times 10^{-10}$) and fibrous/benign breast tissues ($p < 0.001$). This is expected since β -carotene is primarily stored in fatty tissues.³⁵ The hemoglobin saturation showed a significant decrease in malignant tissues relative to that in nonmalignant (including both fibrous/benign and adipose) tissues ($p < 0.0001$), which is likely due to the oxygen extraction of

Table 4 Results from Wilcoxon rank-sum test on extracted absorption, scattering, and fluorescence properties for malignant versus non-malignant and malignant versus fibrous/benign breast tissues (properties are listed in the order of decreasing p value for differentiating between malignant and nonmalignant tissues; fluorescence properties are marked with *).

Extracted Tissue Properties	Malignant versus Nonmalignant	Malignant versus Fibrous/Benign
F_3 contribution*	$p < 1 \times 10^{-8}$	Not significant
β -carotene concentration (μM)	$p < 1 \times 10^{-7}$	Not significant
F_1 contribution*	$p < 1 \times 10^{-7}$	Not significant
Hemoglobin saturation	$p < 1 \times 10^{-7}$	$p < 1 \times 10^{-4}$
Mean reduced scattering coefficient μ'_s (cm^{-1})	$p < 1 \times 10^{-7}$	$p < 0.05$
F_2 contribution*	$p < 1 \times 10^{-4}$	Not significant
Total hemoglobin concentration (μM)	Not significant	Not significant
Baseline absorption	Not significant	Not significant

rapidly proliferating tumor cells. This property agreed with the findings from our previous studies,^{17,18} and has also been reported in several previous studies using other techniques such as pO_2 measurements^{36,37} and near-IR (NIR) diffuse optical spectroscopy.^{33,38,39} Malignant breast tissues had an increased mean reduced scattering coefficient compared to that of nonmalignant breast tissues, which is also consistent with the findings from earlier studies published by Peters et al.¹⁴ and Ghosh et al.¹⁶

Three fluorescence components were extracted from the MCR analysis of the intrinsic fluorescence spectra. The first component (F_1) has peak fluorescence at an excitation-emission pair of (340, 395) nm, which coincides with the primary excitation-emission maximum of collagen.⁴⁰ The EEM of this component is similar to that reported⁴¹ for collagen type 1. Therefore, this component is likely attributed to collagen fluorescence, and in this study we assign F_1 as the collagen component. Collagen is the structural protein present in tissue extracellular matrix. Certain collagens, especially type 1 collagen, is a major constituent of the dermis and fibrous stroma of breast.⁴² It was shown that in normal breast tissues the fluorescence contribution of the collagen component decreased with increasing adipose tissue content, while it increased with increasing fibro-connective and glandular tissue content (as seen in Table 2). This agrees with the fact that collagen resides primarily in the dense fibrous stroma of the breast.⁴² Taroni et al.⁴³ measured absorption of collagen in healthy breast tissues using time-resolved transmittance spectroscopy, and showed that less fatty tissues are characterized by higher collagen concentration. Results of our study also showed that the collagen component has statistically higher contribution to the fluorescence of malignant and fibrous/benign breast tissues, as compared with that of normal adi-

pose tissues ($p < 1 \times 10^{-6}$). Similar observations were also reported in previous studies using other optical spectroscopy techniques for breast tissue characterization.⁴⁴ Haka et al.⁴⁴ used Raman spectroscopy for the diagnosis of breast cancer, and found that there was increased contribution from collagen in benign and cancerous breast tissues, relative to that in normal breast tissues.

The second component (F_2) displayed strong fluorescence at the emission wavelengths ranging in 450 to 500 nm at excitation wavelengths of 360 to 420 nm. The fluorescence feature is spectrally very similar^{40,41,45} to that of NADH, thus, the primary fluorophore that contributes to this fluorescent component is likely NADH. This component F_2 is thus referred as the NADH component. Like the collagen component, the fluorescence contribution from the NADH component was also statistically higher in malignant and fibrous/benign breast tissues than that in adipose breast tissues. Since NADH is one of the important coenzymes for a large number of metabolic activities in cells, the relative concentration of this fluorophore varies according to the oxidative metabolic status of the cells. The higher fluorescence contribution from NADH component in malignant tissues may result from the increased metabolic activity and oxygen depletion in cancer cells, and thus accumulation of NADH. Uppal and Gupta⁴⁶ carried out an enzymatic measurement of NADH concentration in malignant and normal breast tissues, and found that NADH is significantly higher in malignant tissues as compared with normal breast tissues. In the normal breast, NADH may also increase with the increased metabolism associated with the duct proliferation and secretory activities of the breast lobules, while adipose cells have an indolent metabolism.⁴² Therefore, fluorescence of adipose tissues would be expected to have lower contribution from NADH than that of fibrous/benign breast tissues. This explains the negative correlation observed between the fluorescence contribution of this component and adipose tissue content, as well as the positive correlation observed between this fluorescence component and fibroconnective and glandular tissue content in healthy breast tissues.

The third component (F_3) displayed an excitation-emission maximum at (360, 480) nm. This fluorescence peak or shoulder was observed in the intrinsic fluorescence spectra of the majority of adipose breast tissues. However, to our knowledge there is very limited work discussing the source of this fluorescent component. Possible sources for this fluorescence feature can be FAD or retinol/vitamin A, both reported to have fluorescence emission maxima at 520 nm. We measured the fluorescence EEMs of commercially available FAD (F-6625, Sigma-Aldrich Co.) and retinol acetate (R-7882, Sigma-Aldrich Co.). By comparing the extracted EEM of the third component with those of FAD and retinol, we found noticeable similarity between the third component EEM and that of retinol (Fig. 6). Also the relative fluorescence contribution of the third component was highly correlated with the percent adipose tissues content in the breast tissues ($r=0.83$, $p < 1 \times 10^{-18}$, evaluated on sample set 1, and $r=0.76$, $p < 1 \times 10^{-16}$, evaluated on samples set 2, not evaluated on sample set 3 since the percent tissue composition was not available for this sample set), as well as the β -carotene concentration ($r=0.67$, $p < 1 \times 10^{-16}$, evaluated on combined data sets),

Table 5 Results from the (a) holdout validation and (b) leave-one-out cross validation of a linear SVM classification on the combined data sets (sets 2 and 3) for discriminating malignant from nonmalignant breast tissue samples using (1) absorption and scattering properties only, (2) fluorescence properties only, and (3) combination of fluorescence, absorption and scattering properties that show statistically significant differences between malignant and non-malignant breast tissues.

(a) Holdout Validation						
	(1) Abs. & Scatt. Properties Only (%)		(2) Fluorescence Properties Only (%)		(3) All Significant Properties (%)	
	Training	Testing	Training	Testing	Training	Testing
C rate	86.8±3.1	85.6±3.2	80.1±2.5	78.1±2.5	89.3±3.0	86.5±2.5
Sensitivity	82.6±6.0	81.7±5.2	83.4±8.3	82.6±7.5	87.6±4.8	83.9±5.8
Specificity	90.1±2.7	88.6±5.5	78.7±4.9	75.7±4.9	90.6±3.6	88.6±4.7

(b) Leave-One-Out Cross-Validation						
	(1) Abs. & Scatt. Properties Only (%)		(2) Fluorescence Properties Only (%)		(3) All Significant Properties (%)	
	Training	CV	Training	CV	Training	CV
C rate	86.4±0.5	85.5	80.4±0.6	77.4	86.4±0.6	85.5
Sensitivity	83.4±0.5	83.3	85.2±2.3	81.5	83.3±0.8	81.5
Specificity	88.7±0.6	87.1	76.7±2.1	74.3	88.8±0.7	88.6

The classification rate (C rate), sensitivity and specificity were averaged over the repeated training-and-testing trials (CV, cross-validation).

Table 6 Number of tissue samples and the sample numbers of each tissue type that were misclassified in the SVM classification using the three sets of inputs: (1) absorption and scattering properties only; (2) fluorescence properties only; and (3) combination of fluorescence, absorption, and scattering properties.

Type and Subtype	(1) Abs. & Scatt. Properties Only		(2) Fluorescence Properties Only		(3) All Significant Properties	
Malignant						
IDC	6	(3, 14, 82, 84, 86, 116)	6	(3, 21, 54, 68, 86, 110)	5	(3, 82, 84, 86, 116)
ILC	2	(47, 108)	0		2	(47, 108)
DCIS	0		0	(52)	1	(52)
LCIS	1	(36)	1	(36)	1	(36)
Nonmalignant						
Benign	3	(51, 114, 119)	4	(51, 103, 107, 114)	2	(51, 114)
Fibro glandular	2	(44, 64)	8	(1, 22, 44, 64, 97, 101, 105, 112)	2	(44, 64)
Adipose	3	(26, 69, 74)	3	(74, 94, 118)	2	(69, 74)

The sample number for each of the misclassified tissue samples is listed in parentheses to show samples that were misclassified by more than one algorithm.

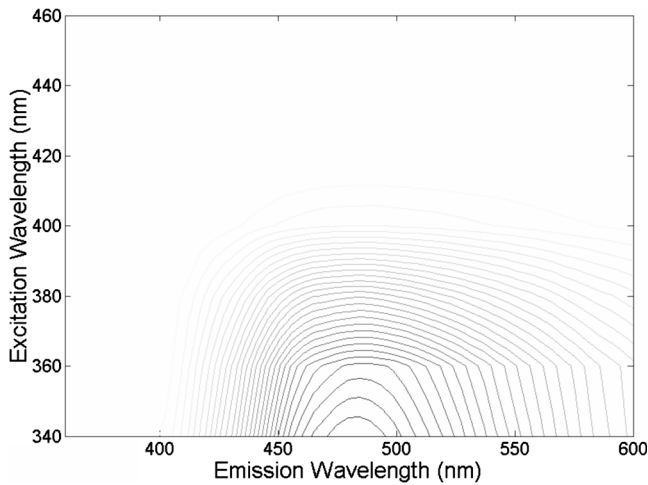


Fig. 6 Fluorescence EEM of retinol acetate (R-7882, Sigma-Aldrich Co.)

which was derived from the Monte-Carlo-inverse-model-based analysis of concomitantly measured diffuse reflectance. β -carotene is a precursor of vitamin A, and is primarily stored in adipose tissues.⁴⁷ Based on these observations and facts, we have tentatively attributed this component to retinol, or vitamin A, and referred to F_3 as the retinol component. A systematic investigation of this fluorescence component may be required in the future in order to fully identify the source and also explore the potential confounding effects of FAD or other factors that may be present in the tissue.

Results from our study suggest that there is a statistically significant increase in fluorescence contribution from retinol component in normal adipose breast tissues compared to that in other tissue types, which may indicate the prevalence of retinol content in normal adipose tissues. Since retinol is fat-soluble, it is primarily present in adipose tissues, and most women carry stores of retinol or vitamin A in their fat cells. Lunetta et al.³⁵ have estimated and compared the retinol concentrations in normal and cancerous breast tissues in breast cancer patients, and found that the retinol concentration in normal breast tissues was slightly higher (on average) than that in malignant breast tissues, however the differences were not statistically significant.

The negative correlation observed between the fluorescence contribution of collagen and NADH components versus the β -carotene concentration may be attributed to fact that collagen and NADH is found predominantly in fibroglandular tissue while β -carotene is found in fatty tissues. The mean reduced scattering coefficient has a positive correlation with the fluorescence contribution of NADH component, while it has a negative correlation with the fluorescence of the retinol component. This may be due to decreasing scattering,^{14,34,48} decreased NADH fluorescence,⁴² and increased retinol fluorescence in adipose tissues. The physiological basis for the negative correlation observed between fluorescence contribution of the collagen component and hemoglobin saturation is not clear. However, fluorescence of the collagen component was found to be prevalent in malignant tissues, which has lower hemoglobin saturation than normal tissues. This may

contribute to the correlation observed between the two variables.

In this study, we extracted the contribution of absorbers, scatterers, and fluorophores in breast tissue and correlated them with histological changes in the normal breast as well as histopathology of the breast. The trends observed in these extracted tissue properties with respect to different tissue types and histopathology findings are consistent with some known facts (such as prevalence of β -carotene and fat in breast tissues) or results reported in other studies, which indicates that the optically determined tissue properties reflect the intrinsic changes in biochemical and physiological properties in breast tissues. However, the limitation of this study is that it was not possible to directly compare the extracted tissue properties to tissue constituent concentrations, because this is a study involving clinical samples, on which disruptive biochemical assays cannot be performed. However, we are currently doing a study to compare the extracted tissue properties to immunohistochemical assays (for example, hypoxia, microvessel density, collagen distribution, etc.) to demonstrate that the optical technique is nondestructively able to quantify biological and morphological information from breast tissues. This will provide a means to directly validate the quantitative physiological aspects of this technique.

The intrinsic fluorescence spectra of each tissue sample were normalized to the integrated intensity over the entire EEM prior to MCR analysis. This normalization removed the intersample variations in the spectral intensity so that the extracted fluorescence contribution only reflected the fractional contributions of individual fluorophores to the fluorescence of each tissue sample. MCR analysis was also carried out on un-normalized intrinsic fluorescence spectra from set 2 only, and it was observed that the relationships of the extracted fluorophore contribution with different tissue types were the same as those observed with the normalized spectra.

The relative fluorescence contribution of all three fluorescing components displayed statistically significant differences between malignant and nonmalignant breast tissues, these differences, however, may be associated with the differences between malignant and adipose tissue only, as a large portion of non-malignant breast samples are adipose tissues. The fluorescence spectra of malignant and fibrous/benign tissue samples shared similar spectral line shapes, and the Wilcoxon rank-sum test did not show statistically significant difference between malignant and fibrous/benign breast tissues in the fluorescence contributions of individual components. In the holdout validation, the classification based on fluorescence contributions alone achieved an average sensitivity and specificity of 83.4 and 78.7%, respectively in training, and 82.6 and 75.7%, respectively, in testing for discriminating malignant from nonmalignant breast tissues. The separation boundary yielded from this classification may discriminate primarily between malignant and normal adipose tissues and a retrospective look at the misclassified samples indicate that most of the misclassified non-malignant samples are fibrous or benign tissues.

Classification using absorption and scattering properties that displayed statistically significant differences between malignant and non-malignant breast tissues provided a slightly decreased sensitivity (82.6% in training and 81.7% in testing using holdout validation) but higher specificity (90.1% in

training and 88.6% in testing using holdout validation) for discriminating breast malignancy, as compared to that achieved using fluorescence properties alone. The improvement to the specificity may primarily be attributed to the inclusion of hemoglobin saturation and mean reduced scattering coefficient, especially the former, which displayed statistically significant differences between malignant and fibrous/benign breast tissues.

The comparable classification performance using fluorescence properties, absorption and scattering properties alone, or both suggest that fluorescence and diffuse reflectance spectra both yield diagnostically useful information for the discrimination of breast malignancy. The retrospective review of the misclassified tissue samples (Table 6) shows that most samples misclassified using fluorescence properties were different from those misclassified using absorption and scattering properties, suggesting the diagnostically useful information yielded from reflectance and fluorescence could be complementary. Although in this study a direct combination of the two sets of tissue properties did not significantly improve the overall classification accuracy, a strategy using absorption and scattering properties and fluorescence properties separately (i.e., sequentially) may have the potential to improve the overall classification.

The model-based approach for feature extraction enables a full exploration of the physiologically relevant information contained in the fluorescence and diffuse reflectance spectra, thus providing a comprehensive understanding of the biochemical, physiological, and morphological changes that take place in the tissue, which has implications in applications such as monitoring tumor response to therapy where both metabolism and hemoglobin oxygenation, for example, are important. Besides providing physiologically meaningful information about the tissue composition and pathology, another advantage of the model-based approach for the analysis of tissue spectra is that it can eliminate the instrument dependency, therefore results obtained using different instruments and probes are directly comparable. In our study, we combined the fluorescence, absorption, and scattering properties extracted independently from two sets of tissue spectra, which were measured with two different instruments and fiber optic probes. The extracted properties were comparable and a statistical *t* test showed that there was no statistically significant difference between the two data sets. This enabled an increased sample size by combining the two data sets.

In this study, the sensitivity and specificity for discriminating breast malignancy were evaluated using two validation methods, i.e., holdout validation and leave-one-out cross-validation, both of which provide an unbiased evaluation of the classification accuracy and the robustness of the classification algorithm. The classification accuracies were consistent across the repeated trials in which training samples were randomly selected from the entire sample set (combined sets 2 and 3). The classification accuracy achieved using holdout validation and leave-one-out cross validation were also comparable.

In conclusion, we presented Monte-Carlo-model-based approaches for the analysis of fluorescence and diffuse reflectance spectra of breast tissues, which enable the extraction of intrinsic fluorescence, absorption, and scattering properties that provide the biochemical and morphological information

about the tissue. The diagnostically useful absorption/scattering properties and fluorescence properties can be used alone or in combination for the discrimination of breast malignancy. It was also demonstrated that the model-based approach has the advantage of eliminating the dependency of fluorescence and diffuse reflectance measurements on the instrument and probe geometry, which makes it a more generalized approach for the analysis of tissue spectra.

Acknowledgments

This work is supported by the National Institutes of Health (NIH) Grant No. 1R01CA100559-01 and the Department of Defense predoctoral traineeship DAMD17-02-1-0628 and W81XWH-05-1-0380.

References

1. C. Zhu, G. M. Palmer, T. M. Breslin, F. Xu, and N. Ramanujam, "The use of a multiseparation fiber optic probe for the optical diagnosis of breast cancer," *J. Biomed. Opt.* **10**(2), 024032 (2005).
2. Y. Yang, E. J. Celmer, M. Zurawska Szczepaniak, and R. R. Alfano, "Excitation spectrum of malignant and benign breast tissues: a potential optical biopsy approach," *Lasers Life Sci.* **7**(4), 249–265 (1997).
3. Y. Yang, A. Katz, E. J. Celmer, M. Zurawska-Szczepaniak, and R. R. Alfano, "Fundamental differences of excitation spectrum between malignant and benign breast tissues," *Photochem. Photobiol.* **66**(4), 518–522 (1997).
4. Y. Yang, A. Katz, E. J. Celmer, M. Zurawska Szczepaniak, and R. R. Alfano, "Optical spectroscopy of benign and malignant breast tissues," *Lasers Life Sci.* **7**(2), 115–127 (1996).
5. G. M. Palmer, C. Zhu, T. M. Breslin, F. Xu, K. W. Gilchrist, and N. Ramanujam, "Comparison of multiexcitation fluorescence and diffuse reflectance spectroscopy for the diagnosis of breast cancer (March 2003)," *IEEE Trans. Biomed. Eng.* **50**(11), 1233–1242 (2003).
6. G. M. Palmer and N. Ramanujam, "Diagnosis of breast cancer using optical spectroscopy," *Med. Laser Appl.* **18**, 233–248 (2003).
7. P. K. Gupta, S. K. Majumder, and A. Uppal, "Breast cancer diagnosis using N2 laser excited autofluorescence spectroscopy," *Lasers Surg. Med.* **21**(5), 417–422 (1997).
8. C.-H. Liu, B. B. Das, W. L. Sha Glassman, G. C. Tang, K. M. Yoo, H. R. Zhu, D. L. Akins, S. S. Lubicz, J. Cleary, R. Prudente, E. J. Celmer, A. Caron, and R. R. Alfano, "Raman, fluorescence, and time-resolved light scattering as optical diagnostic techniques to separate diseased and normal biomedical media," *J. Photochem. Photobiol., B* **16**(2), 187–209 (1992).
9. S. K. Majumder, P. K. Gupta, B. Jain, and A. Uppal, "UV excited autofluorescence spectroscopy of human breast tissues for discriminating cancerous tissue from benign tumor and normal tissue," *Lasers Life Sci.* **8**(4), 249–264 (1999).
10. I. J. Bigio and J. R. Mourant, "Ultraviolet and visible spectroscopies for tissue diagnostics: fluorescence spectroscopy and elastic-scattering spectroscopy," *Phys. Med. Biol.* **42**(5), 803–814 (1997).
11. R. R. Alfano, B. B. Das, J. Cleary, R. Prudente, and E. J. Celmer, "Light sheds light on cancer—distinguishing malignant tumors from benign tissues and tumors," *Bull. N. Y. Acad. Med.* **67**(2), 143–150 (1991).
12. S. V. Pushkarev, S. A. Naumov, S. M. Vovk, V. A. Volovodenko, and V. V. Udut, "Application of laser fluorescence spectroscopy and diffuse reflection spectroscopy in diagnosing the states of mammary gland tissue," *Optoelectron. Instrum. Data. Process.* **2**, 71–76 (1999).
13. I. J. Bigio, S. G. Bown, G. Briggs, C. Kelley, S. Lakhani, D. Pickard, P. M. Ripley, I. G. Rose, and C. Saunders, "Diagnosis of breast cancer using elastic-scattering spectroscopy: preliminary clinical results," *J. Biomed. Opt.* **5**(2), 221–228 (2000).
14. V. G. Peters, D. R. Wyman, M. S. Patterson, and G. L. Frank, "Optical properties of normal and diseased human breast tissues in the visible and near infrared," *Phys. Med. Biol.* **35**(9), 1317–1334 (1990).
15. Y. Yang, E. J. Celmer, J. A. Koutcher, and R. R. Alfano, "UV reflectance spectroscopy probes DNA and protein changes in human breast tissues," *J. Clin. Laser Med. Surg.* **19**(1), 35–39 (2001).

16. N. Ghosh, S. K. Mohanty, S. K. Majumder, and P. K. Gupta, "Measurement of optical transport properties of normal and malignant human breast tissue," *Appl. Opt.* **40**(1), 176–184 (2001).
17. C. Zhu, G. M. Palmer, T. M. Breslin, J. Harter, and N. Ramanujam, "Diagnosis of breast cancer using diffuse reflectance spectroscopy: comparison of a Monte Carlo versus partial least squares analysis based feature extraction technique," *Lasers Surg. Med.* **38**(7), 714–724 (2006).
18. G. M. Palmer, C. Zhu, T. M. Breslin, F. Xu, K. W. Gilchrist, and N. Ramanujam, "Monte Carlo-based inverse model for calculating tissue optical properties. Part II: application to breast cancer diagnosis," *Appl. Opt.* **45**(5), 1072–1078 (2006).
19. G. M. Palmer and N. Ramanujam, "Monte Carlo based model to extract intrinsic fluorescence from turbid media: theory and phantom validation," *J. Biomed. Opt.* **13**, 024017 (2008).
20. Q. Zhang, M. G. Muller, J. Wu, and M. S. Feld, "Turbidity-free fluorescence spectroscopy of biological tissue," *Opt. Lett.* **25**(19), 1451–1453 (2000).
21. N. N. Zhadin and R. R. Alfano, "Correction of the internal absorption effect in fluorescence emission and excitation spectra from absorbing and highly scattering media: theory and experiment," *J. Biomed. Opt.* **3**(2), 171–186 (1998).
22. J. Wu, M. S. Feld, and R. Rava, "Analytical model for extracting intrinsic fluorescence in turbid media," *Appl. Opt.* **32**(19), 3585–3595 (1993).
23. N. C. Biswal, S. Gupta, N. Ghosh, and A. Pradhan, "Recovery of turbidity free fluorescence from measured fluorescence: an experimental approach," *Opt. Express* **11**(24), 3320–3331 (2003).
24. C. M. Gardner, S. L. Jacques, and A. J. Welch, "Fluorescence spectroscopy of tissue: recovery of intrinsic fluorescence from measured fluorescence," *Appl. Opt.* **35**(10), 1780–1792 (1996).
25. M. G. Muller, I. Georgakoudi, Q. Zhang, J. Wu, and M. S. Feld, "Intrinsic fluorescence spectroscopy in turbid media: disentangling effects of scattering and absorption," *Appl. Opt.* **40**(25), 4633–4646 (2001).
26. G. M. Palmer and N. Ramanujam, "Monte-Carlo-based model for the extraction of intrinsic fluorescence from turbid media," *J. Biomed. Opt.* **13**(2), 024017 (2008).
27. G. M. Palmer and N. Ramanujam, "Monte Carlo-based inverse model for calculating tissue optical properties. Part I: theory and validation on synthetic phantoms," *Appl. Opt.* **45**(5), 1062–1071 (2006).
28. R. Huang and S. Jacques, "Skin optics summary" (1998), <http://omlc.ogi.edu/news/jan98/skinoptics.html>.
29. F. P. Bolin, L. E. Preuss, R. C. Taylor, and R. J. Ference, "Refractive index of some mammalian tissues using a fiber optic cladding method," *Appl. Opt.* **28**(12), 2297–2303 (1989).
30. J. R. Mourant, J. P. Freyer, A. H. Hielscher, A. A. Eick, D. Shen, and T. M. Johnson, "Mechanisms of light scattering from biological cells relevant to noninvasive optical-tissue diagnostics," *Appl. Opt.* **37**(16), 3586–3593 (1998).
31. R. Graaff, M. H. Keolink, F. F. M. de Mul, W. G. Zijlstra, A. C. M. Dassel, and J. G. Aarnoudse, "Condensed Monte Carlo simulations for the description of light transport," *Appl. Opt.* **32**(4), 426–434 (1993).
32. R. Tauler, "Multivariate curve resolution, MCR-ALS command line toolbox," (2006), <http://www.ub.es/gesq/mcr/mcr.htm>.
33. A. E. Cerussi, A. J. Berger, F. Bevilacqua, N. Shah, D. Jakubowski, J. Butler, R. F. Holcombe, and B. J. Tromberg, "Sources of absorption and scattering contrast for near-infrared optical mammography," *Acad. Radiol.* **8**(3), 211–218 (2001).
34. T. Durduran, R. Choe, J. P. Culver, L. Zubkov, M. J. Holboke, J. Giammarco, B. Chance, and A. G. Yodh, "Bulk optical properties of healthy female breast tissue," *Phys. Med. Biol.* **47**(16), 2847–2861 (2002).
35. J. M. Lunetta, R. A. Zulim, S. R. Dueker, Y. Lin, V. Flaig, P. D. Schneider, B. M. Wolfe, and A. J. Clifford, "Method for the simultaneous determination of retinol and beta-carotene concentrations in human tissues and plasma," *Anal. Biochem.* **304**(1), 100–109 (2002).
36. W. Mueller-Klieser, K. H. Schlenger, S. Walenta, M. Gross, U. Karbach, M. Hoeckel, and P. Vaupel, "Pathophysiological approaches to identifying tumor hypoxia in patients," *Radiother. Oncol.* **20**(Suppl 1), 21–28 (1991).
37. P. Vaupel, K. Schlenger, C. Knoop, and M. Hockel, "Oxygenation of human tumors: evaluation of tissue oxygen distribution in breast cancers by computerized O₂ tension measurements," *Cancer Res.* **51**(12), 3316–3322 (1991).
38. B. J. Tromberg, N. Shah, R. Lanning, A. Cerussi, J. Espinoza, T. Pham, L. Svaasand, and J. Butler, "Non-invasive in vivo characterization of breast tumors using photon migration spectroscopy," *Aquacultural Eng.* **2**(1–2), 26–40 (2000).
39. D. Grosenick, K. T. Moesta, H. Wabnitz, J. Mucke, C. Stroszcynski, R. Macdonald, P. M. Schlag, and H. Rinneberg, "Time-domain optical mammography: initial clinical results on detection and characterization of breast tumors," *Appl. Opt.* **42**(16), 3170–3186 (2003).
40. N. Ramanujam, "Fluorescence spectroscopy *in vivo*," in *Encyclopedia of Analytical Chemistry*, R. Meyers, Ed., pp. 20–56, John Wiley and Sons, Ltd., Chichester, UK (2000).
41. I. Georgakoudi, B. C. Jacobson, M. G. Muller, E. E. Sheets, K. Badizadegan, D. L. Carr-Locke, C. P. Crum, C. W. Boone, R. R. Dasari, J. Van Dam, and M. S. Feld, "NAD(P)H and collagen as *in vivo* quantitative fluorescent biomarkers of epithelial precancerous changes," *Cancer Res.* **62**(3), 682–687 (2002).
42. S. Thomsen and D. Tatman, "Physiological and pathological factors of human breast disease that can influence optical diagnosis," *Ann. N.Y. Acad. Sci.* **838**, 171–193 (1998).
43. P. Taroni, D. Comelli, A. Pifferi, A. Torricelli, and R. Cubeddu, "Absorption of collagen: effects on the estimate of breast composition and related diagnostic implications," *J. Biomed. Opt.* **12** (1), 014021 (2007).
44. A. S. Haka, K. E. Shafer-Peltier, M. Fitzmaurice, J. Crowe, R. R. Dasari, and M. S. Feld, "Diagnosing breast cancer by using Raman spectroscopy," *Proc. Natl. Acad. Sci. U.S.A.* **102**(35), 12371–12376 (2005).
45. T. G. Scott, R. D. Spencer, N. J. Leonard, and G. Weber, "Synthetic spectroscopic models related to coenzymes and base pairs. V. Emission properties of NADH. Studies of fluorescence lifetimes and quantum efficiencies of NADH, AcPyADH, [reduced acetylpyridineadenine dinucleotide] and simplified synthetic models," *J. Am. Chem. Soc.* **92**(3), 687–695 (1970).
46. A. Uppal and P. K. Gupta, "Measurement of NADH concentration in normal and malignant human tissues from breast and oral cavity," *Biotechnol. Appl. Biochem.* **37**(Pt. 1), 45–50 (2003).
47. Medline Plus Medical Encyclopedia online, <http://www.nlm.nih.gov/medlineplus/ency/article/002400.htm>.
48. S. Srinivasan, B. W. Pogue, S. Jiang, H. Dehghani, C. Kogel, S. Soho, J. J. Gibson, T. D. Tosteson, S. P. Poplack, and K. D. Paulsen, "Interpreting hemoglobin and water concentration, oxygen saturation, and scattering measured in vivo by near-infrared breast tomography," *Proc. Natl. Acad. Sci. U.S.A.* **100**(21), 12349–12354 (2003).